JOURNAL OF SYNCHROTRON RADIATION

Volume 26 (2019)

Supporting information for article:

M-BLANK: a program for the fitting of X-ray fluorescence spectra

Andrew M. Crawford, Aniruddha Deb and James E. Penner-Hahn

Supporting Information

M-Blank: A program for fitting of x-ray fluorescence spectra

Andrew M. Crawford, Aniruddha Deb, James E. Penner-Hahn*

Abstract: The x-ray fluorescence data from x-ray microprobe or nanoprobe measurements must be fitted to obtain reliable elemental maps. The most common approach to fitting is to initially remove a per-pixel baseline. Using x-ray fluorescence data of yeast and glial cells, we demonstrate that per pixel baselines can result in significant, systematic errors in quantitation and that significantly improved data can be obtained by calculating an average blank spectrum and subtracting this from each pixel.

Experimental Procedures

Cultured yeast cells were resuspended in deionized water at a final OD_{600} of 0.5 and 1 µl was applied to a silicon nitride sample window. Samples were allowed to settle for 5 minutes prior to being plunge-frozen using either a Leica CPC plunge-freezing apparatus and liquid ethane at -165 °C, or an Electron Microscopy Supplies EMS-002 plunge-freezing apparatus using liquid propane at -175 °C. Samples were subsequently lyophilized to dryness.

XRF measurements were carried out at Sector 2 of the Advanced Photon Source at Argonne National Laboratory with 150 x 150 nm spatial resolution using the instrument at station 2-ID-D and an excitation energy of 10 keV. Acquisition times ranged from 1.5 to 6 seconds per pixel. A similar approach was used to measure data for thin-film calibration standards NBS 1832 and 1833.

Rat glial C6 cells were cultured in DMEM/F12 media supplemented with 10% FBS on silicon nitride windows (Norcada, Canada) and fixed as previously described[1]. XRF measurements were carried out at Sector 2 of the Advanced Photon Source at Argonne National Laboratory with 250 x 250 nm spatial resolution using the instrument at station 2-ID-D with an excitation energy of 14.25 keV and acquisition times of 0.4 seconds $pixel^{-1}$. A similar approach was used to measure data for thin-film calibration standards NBS 1832 and 1833.

Calculation Details

Identifying Blank Pixels. Separation of cell and non-cell pixels in each image was performed in an automated iterative process that began by using the potassium Kα emission line to generate an approximate image of the cell. An ROI centered on potassium gave an estimate of the potassium counts for each pixel. All pixels with intensities greater than half of the maximum potassium signal were initially defined as "cell" pixels. Each round of iteration began by calculating the mean, $\bar{x}$, and standard deviation, σ, of the non-"cell" pixels. Any pixel with an intensity greater than $\bar{x}$ +2σ which was also contiguous with existing “cell” pixels was defined as "cell", and this process continued until no new pixels were redefined. In a final step any “non-cell” pixel that was surrounded by 8 “cell” pixels was relabeled “cell” as well.

Non-cell pixels were further refined for calculating the blank spectrum by identifying and rejecting any pixel that contained contaminants. These cropped/rejected pixels were identified by fitting the histograms of all the fitted elements from all non-sample pixels to a normal distribution and rejecting all pixels with any elemental intensity greater than 3 standard deviations from its mean. This process repeated until the population of identified pixels became self-consistent.

Determination of Peak Fitting Parameters. As part of the peak fitting, it is necessary to determine the energy and peak shape for each of the fluorescence peaks. Energy calibration defines the relationship between the known fluorescence energies and the detector channel, E_i, giving the maximum intensity for each element. The peak shape was modeled using the modified Gaussian, P, in Eq. (S1) [2].

$$P(i,E) = G(i,E) + S(i,E) + T(i,E) \qquad \text{Eq. (S1)}$$

where G is a Gaussian representing the elemental emission (Eq. (S2)), S is a step (Eq. (S4)) due to electron escape and T is a tail (Eq. (S5)) due to incomplete charge collection. In Eqs. (S4) and (S5), B_i gives the magnitude of the correction and β_i is the broadening of the exponential tail [3].

$$G(i,E) = A_i \exp\left[-\frac{(E - E_i)^2}{2\alpha_i^2}\right] \qquad \text{Eq. (S2)}$$

$$\alpha(i,E) = \left[a_0^2 + (a_1 E_i)\right]^{1/2} \qquad \text{Eq. (S3)}$$

$$S(i,E) = B_i \exp\left[\frac{(E - E_i)^2}{\beta_i}\right] \qquad \text{Eq. (S4)}$$

$$= 0,\ E \geq Ei$$

$$T(i,E) = \frac{B_i}{2} \exp\left[\frac{E - E_i}{\beta_i}\right] \exp\left[\frac{\alpha_i^2}{2\beta_i^2}\right] erfc\left[\frac{E - E_i}{\alpha_i\sqrt{2}} + \frac{\alpha_i}{\beta_i\sqrt{2}}\right] \qquad \text{Eq. (S5)}$$

Using Eq. (S1) rather than a simple Gaussian peak shape increases the number of fitted peak-shape parameters from 2 per element to 4 per element (E_i, α_i, B_i, and β_i). To avoid over-parameterization, all 4 parameters were constrained to be quadratic functions of energy, thus giving a total of 12 fitted parameters.

Typically the peak shape parameters (α_i, β_i, and B_i) and the energy calibration parameter, E_i, are determined by fitting the fluorescence signal from a calibration standard. However, standards and samples often have quite different count rates, and count-rate related distortions can alter the peak-shape and energy calibration parameters. For this reason, M-Blank uses the sum of all “cell” pixels

minus the weighted sum of all blank pixels to define the energy calibration and peak-shape parameters for samples; these parameters are then optimized for standards by allowing only the detector energy calibration and the detector response function (Eq. (S3)) to float while constraining all other parameters. This gives more reliable peak shape parameters because only the fluorescence peaks need to be fit and there is no need to subtract an *ad hoc* smooth baseline. The peak amplitude parameters were converted to counts/areal mass by spectra from the NBS 1832 and NBS 1833 standards (National Institute of Standards & Technology).

Once the peak-shape and energy calibration parameters were defined, each scan was processed by first calculating a scan-specific blank (the mean spectrum of all non-cell pixels from that image) and subtracting this from each pixel. This difference was then fit using linear least squares to give the areal concentration (μg cm^{-2}) of each element at each pixel.

Comparison with other quantitation methods. In order to compare the results from blank corrected fitting with those from per-pixel baseline corrected fitting, we fit the data both using M-BLANK and using MAPS[4]. The per-pixel baselines calculated in MAPS were subtracted from the raw XRF spectra (that is, the MAPS baselines were used in lieu of the blank that would normally be used in M-BLANK). The resulting difference was then fit, in M-BLANK, using non-negativity constraints to ensure non-zero apparent elemental concentrations. The resulting fitted signal corresponds to S+F in Eq. (3). In order to recover the signal, S, the background fluorescence, F, was removed by calculating the average XRF for the non-cell regions and subtracting this from each cell pixel.While baseline and blank subtraction should give equivalent results, we find significant differences, particularly for lower atomic-number elements (see text).

Importantly, it must noted that although the per-pixel baseline corrected data presented in this manuscript were obtained using baselines generated in MAPS, we find similar results using baselines from PyMCA and PyXRF (data not shown)..

Determination of sub-populations for Figure 3. Scatter plots of $\frac{XRF_{baseline\ corrected}}{XRF_{blank\ corrected}}$ vs $\frac{XRF_{blank\ corrected}}{max(XRF_{blank\ corrected})}$ show several nested subpopulations. These were initially assigned manually to one of seven subpopulations. These were then each fit using Equation 6. Each point was then reassigned to the subpopulations for which the fit gave the minimum Cartesian distance to the point. This process repeated until all populations became self-consistent.

In order to arrive at an estimate of the range of validity of the baseline subtraction, we determiend the minimum concentration (in reduced units x_i) for which the baseline subtracted value was within 5% of the blank corrected value. This is equivalent to determine the x_i values for whichy_i iswithin 5% of m (the ratio of empirical calibration slopes). For nonzero λ, Eq. (6) can be rewritten to solve for x_i where y_i is within 5% of m (e.g., for sulfur, Fig. 3A inset table).

For $\lambda > 0$, (i.e., asymptotically approaching m from below) Eq. (7) is derived as follows:

$m-\lambda/x_i \geq 0.95m$

$0.95 \leq (m-\lambda/x_i)/m$

$0.95 \leq 1-\lambda/(x_i\, m)$

$0.05 \leq \lambda/(x_i\, m)$

$x_i \geq \lambda/(0.05m)$

$x_i \geq 20\lambda/m$

For $\lambda < 0$, (i.e., asymptotically approaching m from above):

$m-\lambda/x_i \leq 1.05m$

$1.05 \geq (m-\lambda/x_i)/m$

$1.05 \geq 1-\lambda/(x_i\, m)$

$0.05 \geq -\lambda/(x_i\, m)$

$x_i \geq -\lambda/(0.05m)$

$x_i \geq -20\lambda/m$

Non-negativity constraints

For baseline corrected data, one can constrain the least-squares fits to be non-negative. While this is not required when using per-pixel baselines, and although non-negativity constraints come at the cost of signicantly slower fitting, they are nevertheless widely used because they have the potential to avoid parameter correlation. That is, if peaks are constrained to be non-negative, then there is no risk that the fit may find a non-physical minimum with alternating large positive and large negative amplitudes for adjacent peaks, when in fact, there is no measured signal.

Non-negativity constraints should never be employed when using blank subtraction. In a photon-counting method such as XRF imaging, the measured data is, by definition, an integer number of counts. However, our approach of averaging the measured blank signal over a large number of pixels almost inevitably gives a measured blank that is some fractional number of counts/pixel. The low amplitude of the per-pixel signals means that there are often pixels that have no XRF counts in a given energy bin. When the blank is subtracted from these pixels, the resulting background-corrected counts will be negative. As a consequence, fits with M-BLANK, when using blank correction, should not include non-negativity constraints, but rather allow for the possibility of either positive or negative apparent concentrations for each element. If an element is not present above the background level, the fitted counts should be distibuted evenly around zero. We have not observed difficulties from parameter correlation in our fits.

Supplemental Figures

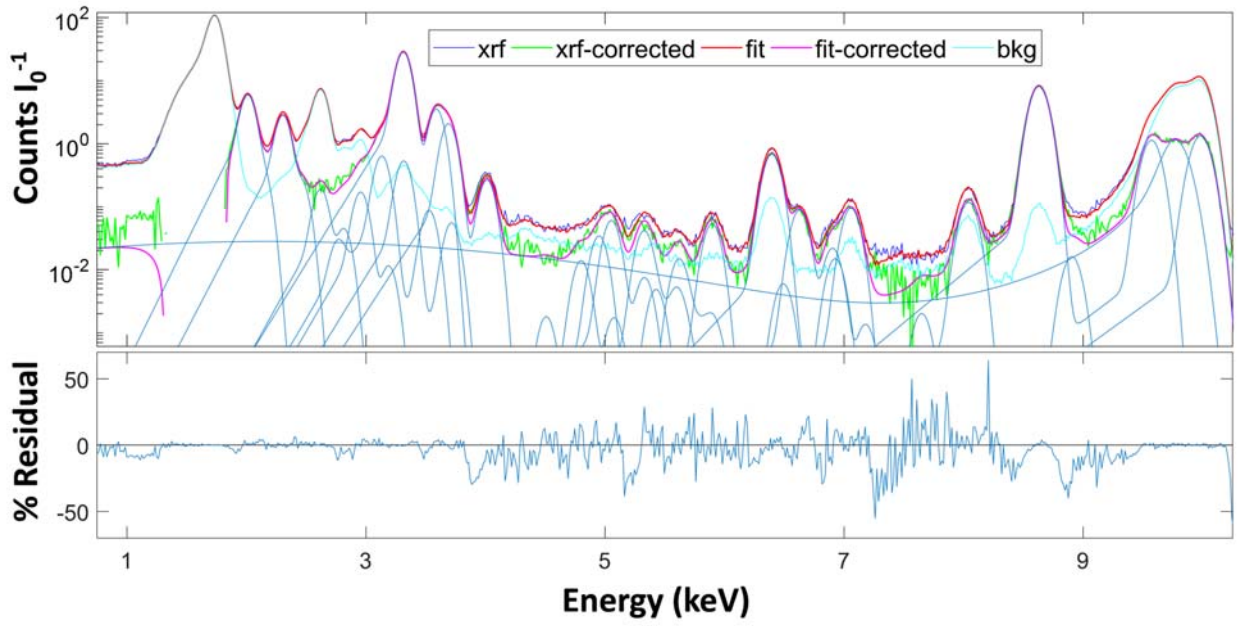

Figure S1. Representative fit (top) and residual (bottom) of the XRF emission from a yeast sample. The sample blank is shown in cyan (bkg).

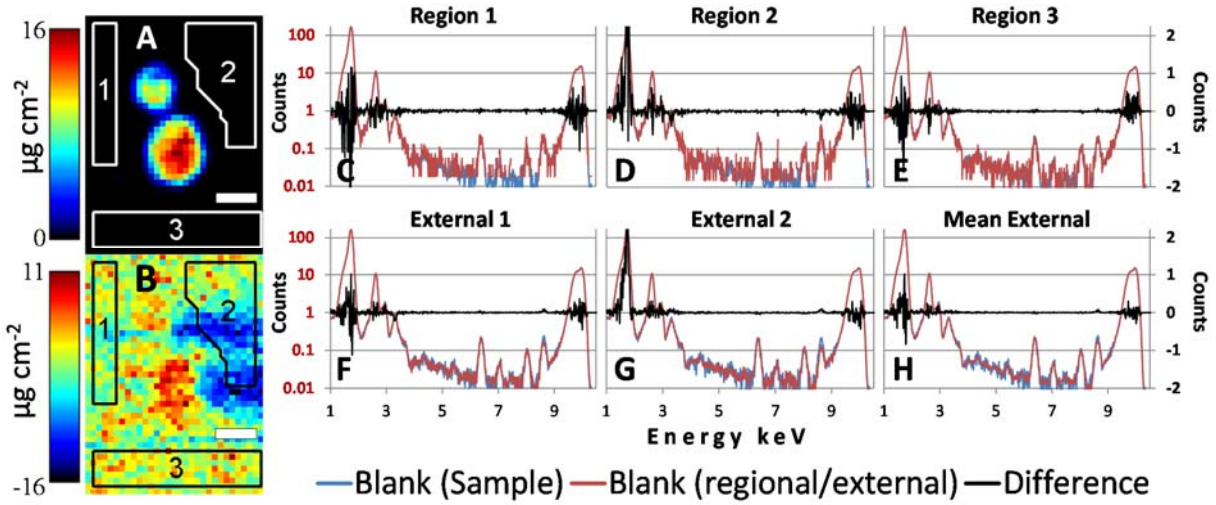

Figure S2. Characterization of blanks regions. A) Potassium distribution, as determined from the fitted K emission (scale bar = 2 μm). Three different blank regions have been identified, marked by numbers **1**-**3**. B) Silicon distribution, as determined from the fitted K emission, showing the heterogeneity in the silicon signal. C-H) Comparison of measured signal in blank region (red line) with the estimated blank signal (blue line) from the full set of spectra from all non-sample pixels from the data corresponding to images A and B. The difference is shown in black (right hand scale). The measured blank is from region **1** (C), **2** (D) or **3** (E). F&G) External blanks (red line) were calculated from two additional images of yeast cells fixed on Si_3N_4, showing the reproducibility from sample to sample. The external blank in H is taken as the average of the blank region from 6 samples.

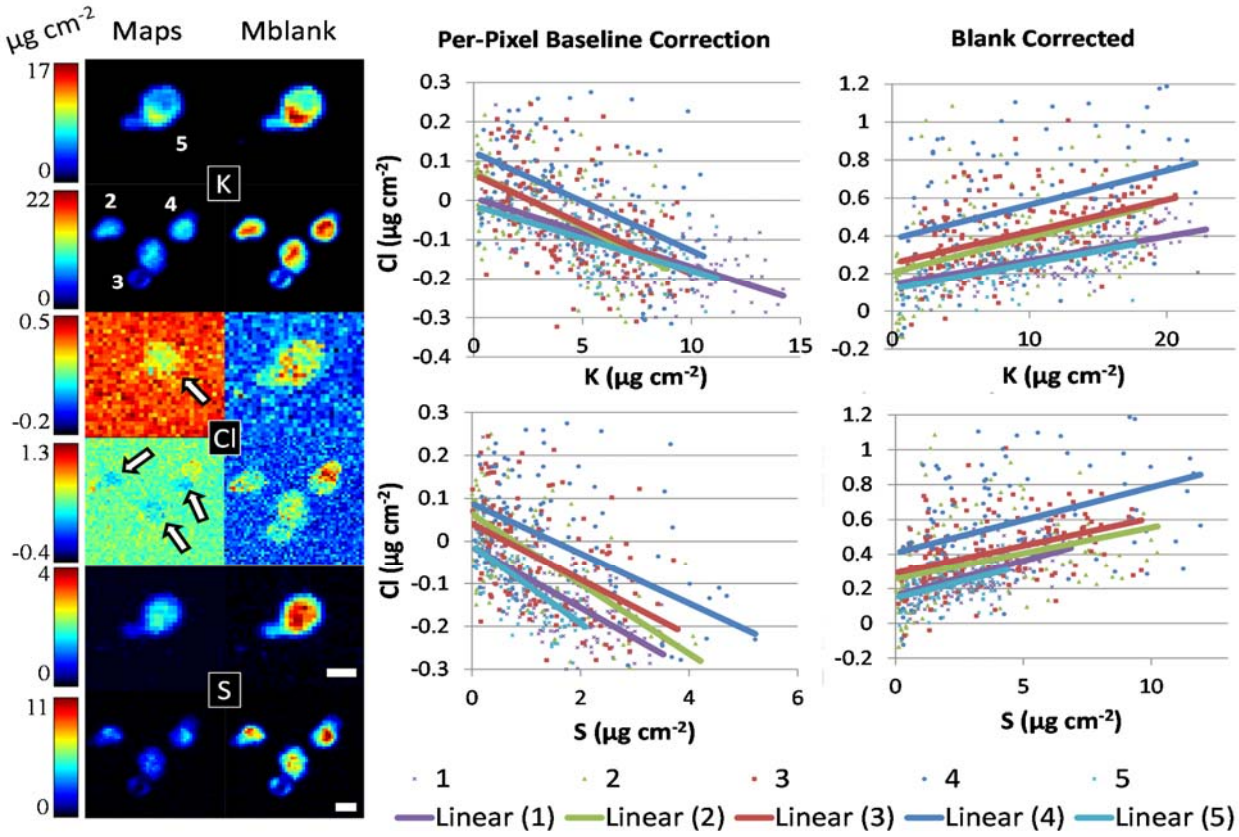

Figure S3. Elemental correlation for S, Cl, and K. Left – Two image sets containing 4 cells (labelled 2-5) showing distributions of K (top), Cl (middle), and S (bottom) as determined using a per-pixel baseline (MAPS; Left 6 images) or blank correction (M-Blank; Right 6 images). The arrows in the Cl images indicate the regions that give apparent negative cellular chlorine. Right – Per-pixel elemental correlations for the cell pixels from 1 (shown in Figure 1, main text) and cells 2-5 along with linear fits for each cell's correlation. Intensity bars are in units of µg cm^{-2}. Length scale bars = 2 µm.

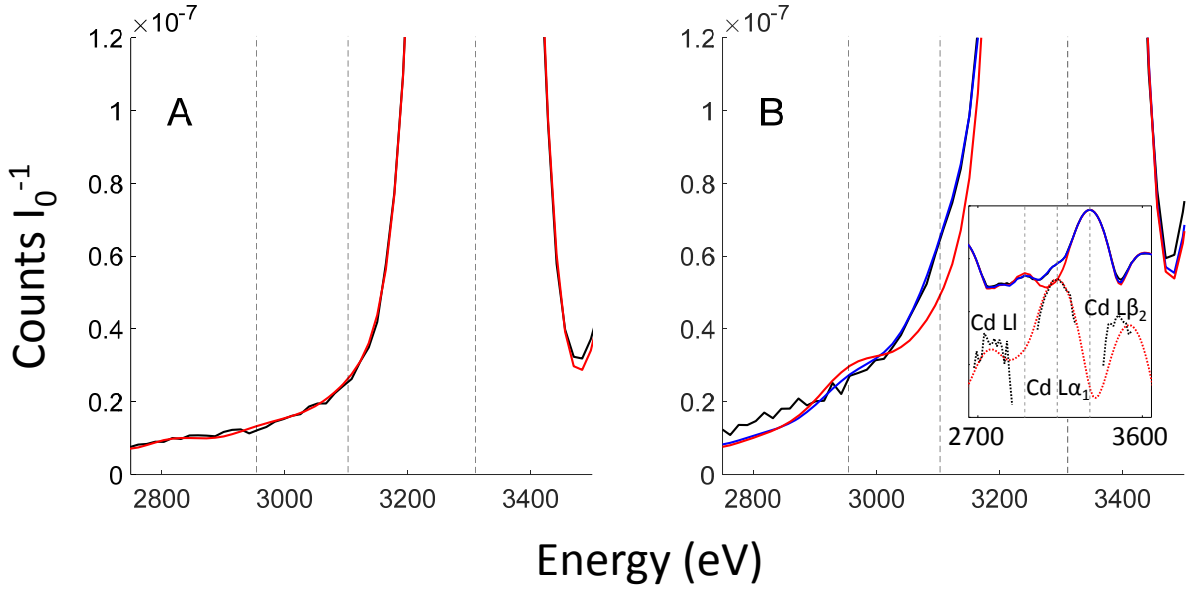

Figure S4. Integrated emission spectrum for cell pixels in samples of yeast that had been incubated with 0 mM Cd (A) or 250 mM Cd (B; inset is log scale for y). Vertical lines, from left to right, mark the energies of the argon Ka, cadmium La, and potassium Ka lines. Black) Experimental spectrum; Red) Best fit without including the Cd La1 (L3M5, 3134 eV) or Lb1 (L2M4, 3317 eV) lines . For the Cd containing sample, this fit compensates for the absence of the Cd lines by increasing the amplitude of the argon and potassium peaks by 41 and 1 percent, respectively. Blue) Best fit for samples incubated with 250 mM Cd when the Cd La1 and Lb1 lines are included. Dashed Black) Residual when fit without including the Cd La1 or Lb1 (L2M4, 3317 eV) lines. Dashed Red) Fitted Cd L3 emissions showing Cd La1 and including Cd Ll (L3M1, 2767 eV) and Cd Lb2 (L3N5, 3528 eV). Fitting parameters for A and B were identical and the fitting of A with and without including the Cd L lines yielded identical results.

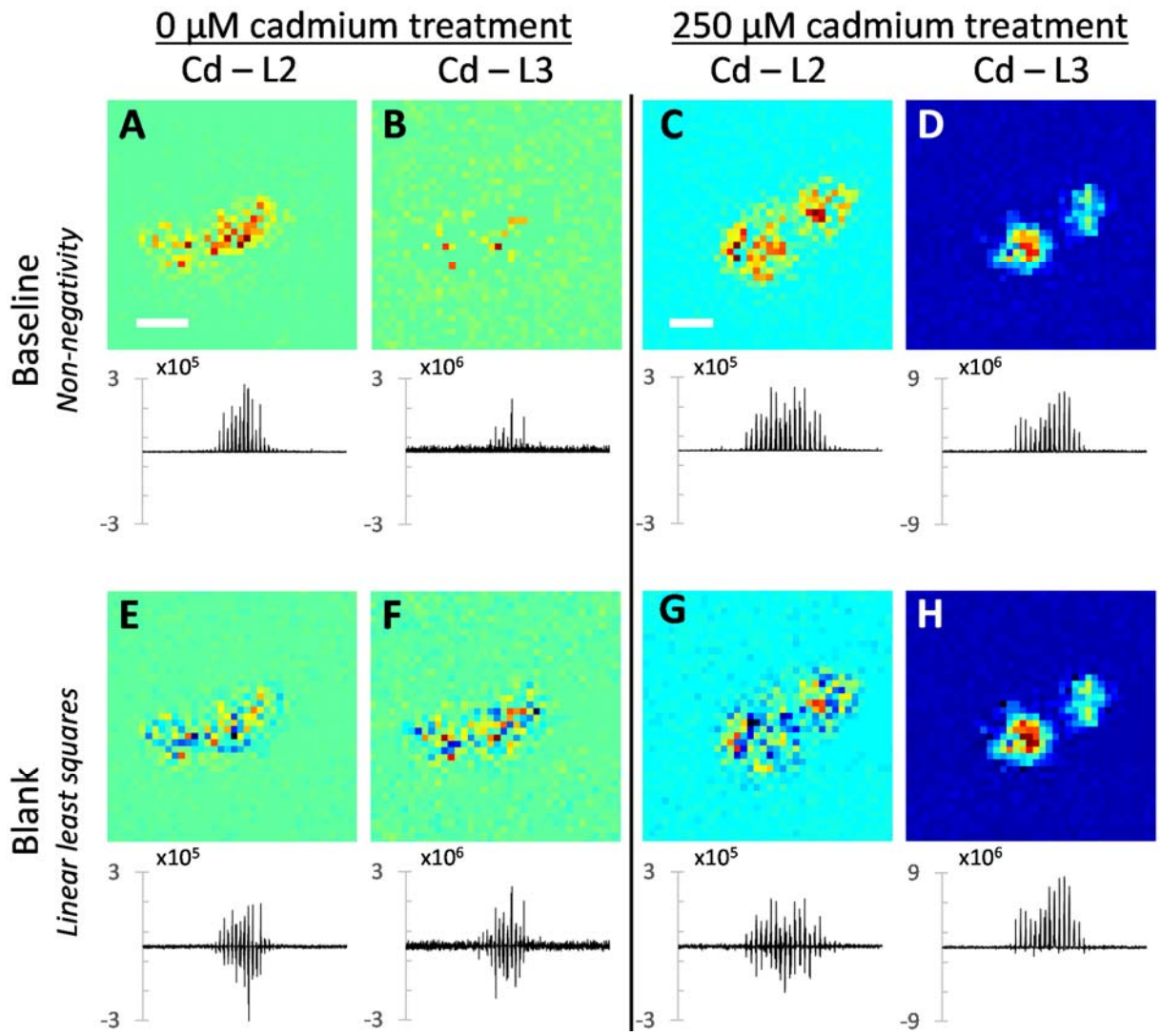

Figure S5. Images showing the fitted peak heights for the cadmium "L2" lines (L_2-N_4 or $L\gamma_1$ at 3710 eV and L_2-M_4 or $L\beta_1$ at 3319 eV) inpanels A, C, E, and G and fits for the cadmium "L3" lines (L_3-N_5 or $L\beta_2$ at 3525 eV; L_3-M_5 or $L\alpha_1$ at 3134 eV; L_3-M_4 or $L\alpha_2$ at 3131 eV; and L_3-M_1 or L_ℓ at 2767 eV) in panels B, D, F, and H. Below each image is a line plot showing the fitted peak intensity for each pixel, with pixels numbered in rows starting from upper left and running to lower right. Panels A-D are the fits obtained using a per-pixel baseline and non-negativity constraints. Panels E-G are the fits obtained using blank correction in M-BLANK with an unconstrained non-linear least-squares fit. For the Cd containing samples, both approaches give reasonable, quantitatively similar fits for the L3 lines (Panels D and H) and both fail to give meaningful fits for the L2 lines (the most intense L2 line, $L\beta_1$ overlaps almost perfectly with the much more intense potassium line; 3317 vs 3314 eV, Panels C and G). However, the failure modes are different. For M-BLANK it is apparent that the L2 intensities are uniformly distributed around zero. That is, this cadmium L2 is indistinguisable from noise in the presence of the intense potassium Kα signal. In contrast, non-negativity constraints mean that fits to the cadmium L2 appear to give a signal, albeit one that is ~15 fold weaker than it should be based on the observed cadmium L3 intensities. While this is of little consequence for samples that contain cadmium, it suggests a false positive for the cadmium free sample (Panels A and B). In contrast, M-BLANK gives the expected net-zero signal for these samples (Panels E and F). Distance scale bars measure 2 microns.

Video

An illustrative comparison of the blank used in M-Blank with per-pixel baselines used elsewhere is contained in a video at https://drive.google.com/file/d/11Np_K7TZPtIzgAxZfg4xSecjL9JWhDVV/view. The first ~26 seconds shows the raw data as the program rasters through all the blank pixels (identified as described above). The signal at each pixel (light blue) is shown along with the per-pixel baselines (light grey) and the accumulating average blank (red). At 26 seconds, the full energy spectrum of the blank has emerged, showing that there is a background signal for iron, copper, and zinc with Kα peak intensities of 0.3, 0.1, and 0.2 counts/pixel, respectively. From 26 seconds to 38 seconds the video rasters through the cell pixels and calculates the mean cell fluorescence spectrum (orange), cumulatively. For each pixel, the calculated per-pixel baselines are shown for comparison with the measured blank. From 38 seconds to 56 seconds the video rasters a second time through the non-sample pixels, this time accumulating the mean signal only for the pixels that were rejected (yellow; see above) when identifying blank pixels.

References

[1] E. A. Carter, B. S. Rayner, A. I. McLeod, L. E. Wu, C. P. Marshall, A. Levina, J. B. Aitken, P. K. Witting, B. Lai, Z. H. Cai, S. Vogt, Y. C. Lee, C. I. Chen, M. J. Tobin, H. H. Harris, P. A. Lay, *Molecular Biosystems* **2010**, *6*, 1316-1322.

[2] R. E. Van Grieken, A. A. Markowicz, in *Practical Spectroscopy*, 2 ed., Marcel Dekker, **2002**, p. 287.

[3] J. L. Campbell, J. A. Maxwell, *Nucl. Instruments Methods Phys. Res. B* **1997**, *129*, 297-299.

[4] S. Vogt, *J. Phys. IV France* **2003**, *104*, 635-638.

Author Contributions

A.M.C. wrote all software, and performed all fitting and formal analyses. A.M.C, A.D., and J.E.P.-H. participated in investigation and conceptual development. J.E.P.-H. provided funding acquisition, project administration. A.M.C. and J.E.P.-H. were responsible for data curation. A.M.C. and J.E.P.-H. wrote the manuscript.